Magnetic Interaction between Surface-Engineered Rare-Earth Atomic Spins

Chiung-Yuan Lin,[1] Jheng-Lian Li,[1,2] Yao-Hsien Hsieh,[1] Keng-Liang Ou,[2,3] and B. A. Jones[4]

[1]*Department of Electronics Engineering and Institute of Electronics, National Chiao Tung University, Hsinchu, Taiwan*
[2]*Research Center for Biomedical Devices, Taipei Medical University, Taipei, Taiwan*
[3]*College of Oral Medicine, Taipei Medical University, Taipei, Taiwan*
[4]*IBM Almaden Research Center, San Jose, California 95120-6099, USA*

(Received 9 March 2012; revised manuscript received 1 May 2012; published 22 June 2012; corrected 20 July 2012)

We report the *ab-initio* study of rare-earth adatoms (Gd) on an insulating surface. This surface is of interest because of previous studies by scanning tunneling microscopy showing spin excitations of transition-metal adatoms. The present work is the first study of rare-earth spin-coupled adatoms, as well as the geometry effect of spin coupling and the underlying mechanism of ferromagnetic coupling. The exchange coupling between Gd atoms on the surface is calculated to be antiferromagnetic in a linear geometry and ferromagnetic in a diagonal geometry. We also find that the Gd dimers in these two geometries are similar to the nearest-neighbor and the next-nearest-neighbor Gd atoms in GdN bulk. We analyze how much direct exchange, superexchange, and Ruderman-Kittel-Kasuya-Yosida interactions contribute to the exchange coupling for both geometries by additional first-principles calculations of related model systems.

DOI: 10.1103/PhysRevX.2.021012 Subject Areas: Magnetism, Nanophysics

I. INTRODUCTION

Understanding spin coupling at the nanoscale is important in scaling down magnetic devices such as spintronics and quantum computing devices [1]. During the past years, it has been demonstrated that the scanning tunnelling microscope (STM) is a powerful tool for building and controlling individual nanomagnetic structures, and has a great potential for use in the construction of future nanoscale magnetic devices. Previous studies of engineering individual magnetic atoms on surfaces [2] include exchange coupling between magnetic atoms [3–6], anisotropic spin environments of a single atom or dimer [7–9], and observations of Kondo effects [10,11]. Very recently, atom manipulation using the STM has been able to demonstrate important technological progress such as logic operations entirely based on engineered atomic spins [12] and dense nonvolatile storage of information by an atomic-scale antiferromagnet [13].

Before physicists started using the STM to manipulate and couple magnetic atoms together, chemists had for decades been synthesizing numerous species of molecules that carry giant spins, well-known as molecular magnets [14]. The STM-engineered spins have been found to form a surface molecular network with great similarity to molecular magnets. While the major attention in the field of molecular magnets is mainly focused on those consisting of transition-metal magnetic atoms, very few studies are devoted to rare-earth-based molecular magnets. Moreover, only magnetic anisotropy has been studied for the rare-earth-based molecular magnets [15], not the interatomic spin coupling within such molecules. A similar situation also exists with STM-engineered spins; experimentalists have not yet tried to place rare-earth atoms on surfaces to see how their spins couple to each other.

The rare earths are naturally complex and interesting materials due to the interplay between f- and d-electron magnetism, one tending toward localized and the other toward itinerant magnetism. In bulk, they display complex Ruderman-Kittel-Kasuya-Yosida (RKKY)–based spiral magnetic phases, as well as mixed valence and, when mixed with nonmagnetic atoms, heavy fermion behavior (that is, strongly correlated electron systems with competing superconducting and magnetic phases).

When the individual adatoms or dimers are studied on a partially insulating surface, we likewise expect complex behavior. Gd is a promising candidate for study for several reasons. First, having a half-filled $4f$ shell, it carries a large atomic spin $S = 7/2$, giving Gd magnets in bulk some of the largest magnetic moments (cf. the transition-metal atoms for which Mn has the largest, at $S = 5/2$). An atomic spin this large approaches the quantum-classical border and is likely to give rise to interesting magnetic interactions. The interplay between f and d electrons should also create a pull between itinerant (molecular) magnetism and localized magnetism. Unlike rare earths with nearly empty or full f shells, Gd does not show any mixed valent behavior in bulk, being in the middle of its row in the periodic table, which should also enhance its magnetic interactions. In particular, RKKY interactions have not usually been seen with STM studies of d-electron materials on insulating surfaces. One goal of this work with Gd is to see whether the strong RKKY

interactions present in bulk will carry over to pairs of interacting Gd atoms on an insulating surface.

In this study, we present a new method for separating out the components of the spin coupling between two magnetic atoms on an insulating surface. We are able to separately determine the RKKY, superexchange, and direct exchanges between the two, and, in addition, to show the microscopic source of the different interactions. The presence of superexchange was expected from previous studies, but the presence and size of both direct exchange and RKKY effect in these systems are surprising results of our research.

A common substrate among previous atom-manipulation studies using STM has been a copper-nitride insulating monolayer on top of a Cu(100) surface [3,7,9–11,13] (to be referred to herein as the CuN surface), and we use this same surface and substrate in our calculations. Gd on such a surface will form Gd-N bonds. Guided by analogies with the related bulk GdN system, we look for two coupling paths for the Gd, one directly across a N and the other diagonal, which is actually the nearest-neighbor (NN) configuration. In bulk, these have opposite signs of exchange coupling (antiferromagnetic vs ferromagnetic, respectively [16,17]). Hence we expect, by changing the binding angles (as opposed to changing primarily the interatomic distance [18]), to tailor the sign of the Gd-Gd spin coupling on the CuN surface, while keeping the spin-interaction magnitude roughly the same. By using our new methodology to understand the source of the coupling, we hope to enable experimentalists to tailor the interactions to be either ferromagnetic or antiferromagnetic, and, in fact, to tune the interactions over a whole range of parametric phase space of the coupling sources, enabling better control of future atomic-scale bits.

Gd has an f shell of $L = 0$ that is expected to exhibit a quite small magnetic anisotropy on surfaces due to small spin-orbit interaction. (In fact, we calculate it to be less than 0.1 meV by turning on the spin-orbit coupling.) Spin coupling and magnetic anisotropy can both contribute to inelastic tunneling spectroscopy using the STM. If both types of excitations exist at the same energy scale, the inelastic tunneling spectra are difficult to analyze. On the other hand, with low anisotropy, one would expect Gd atoms on the CuN surface to yield clean inelastic-tunnelling spectra mainly from the interatomic coupling of their spins. Such an advantage would benefit experimental studies that follow this first-principles investigation.

In this work, we perform first-principles calculations of Gd adatoms on the CuN surface. In some ways, the Gd atoms are similar to the previously studied Mn atoms [7,19] when being deposited on the Cu sites of the CuN surface, i.e., the Gd's nearby N atoms break bounds with their neighboring Cu and form a ''quasi''-molecular structure from the surface. However, the local structures of the Gd atoms on the CuN surface have a well-studied reference system: the GdN bulk. We build two different geometries of the Gd dimers on the surface: one has Gd atoms along the same N row, and the other along two perpendicular N rows. The two geometries mimic the coupling paths of the nearest-neighbor and next-NN (NNN) Gd atoms of the GdN bulk, where the two paths in bulk have ferromagnetic and antiferromagnetic couplings, respectively. We calculate the exchange couplings J of two arrangements of Gd_2/CuN using first-principles Perdew-Burke-Ernzerhof functional [20] plus the Coulomb repulsion parameter (PBE + U), and expect that one of the two types of surface Gd dimers will exhibit ferromagnetism and the other antiferromagnetism.

II. COMPUTATIONAL APPROACHES

In the STM experiments, a copper-nitride monolayer is built between a magnetic atom and the Cu(100) surface [3,7,9–11] to keep the atomic spin away from the screening of its underlying conduction electrons while permitting a sufficient amount of STM tunneling current for probing the spin excitations. To understand the magnetic properties of Gd atoms on the CuN surface, we simulate a single Gd on this surface by first constructing a supercell of five-layer Cu slabs plus eight vacuum layers with the nitrogen atoms snugging in-between half of the vacant sites, and then placing each Gd atom atop the Cu site on the CuN surface within a three-unit cell. We perform density-functional calculations in the all-electron full-potential-linearized augmented-plane-wave basis [21]. A naïve local density approximation (LDA) or generalized gradient approximation (GGA), when being applied to materials composed of rare-earth atoms, generally yields f levels inconsistent with photoemission experiments and needs to be fixed by adding extra on-site Coulomb repulsion to the exchange-correlation functional, the so-called ''density functional theory plus the Coulomb repulsion parameter'' (DFT + U) method [22]. To determine the on-site Coulomb U_f and exchange J_f values of the Gd $4f$ orbitals on the CuN surface, we revisit the GdN bulk system, which mimics very well the local structure of Gd on the CuN surface. The GdN bulk, being a ferromagnetic semiconductor, has been studied experimentally by photoemission and computationally by the ''local spin density approximation plus the Coulomb repulsion parameter'' (LSDA + U) method for its potential application in spintronics. Following previous LSDA + U studies of GdN bulk [16,23], we find that $U_f = 6.7$ eV and $J_f = 0.7$ eV yield the energy difference between the majority-spin Gd $4f$ and N $2p$ states in best agreement with photoemission measurements [24,25]. This set of U_f and J_f are used in our succeeding PBE + U calculations of both the GdN bulk and the Gd dimer on the CuN surface.

The spin couplings along the diagonal and the linear Gd-N-Gd paths of the GdN bulk are well studied in the literature [16,17], where the two Gd atoms along the paths

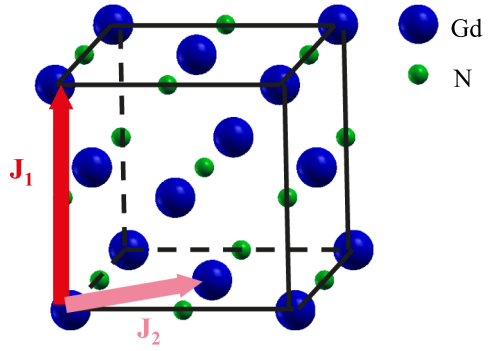

FIG. 1. The unit cell of a GdN bulk. The Gd-to-Gd arrows indicate the NN (diagonal, pink) and next-NN (linear, red) couplings.

are NN and next-NN to each other, respectively, as shown in Fig. 1. The two coupling paths between Gd atoms in a GdN bulk strongly suggest that there are two possible geometries of Gd dimers on the CuN surface: one has Gd-N-Gd along the N-row, and the other in a right angle (two Gd atoms along the diagonal). Previous GdN-bulk studies [16,17] have concluded that the spin couplings between Gd atoms of a GdN bulk along the diagonal and the linear paths are ferromagnetic and antiferromagnetic, respectively. Therefore, we expect the surface Gd dimers in two geometries to have spin couplings that are the same as their counterparts of similar geometries in the GdN bulk, i.e., diagonal (linear) being ferromagnetic (antiferromagnetic).

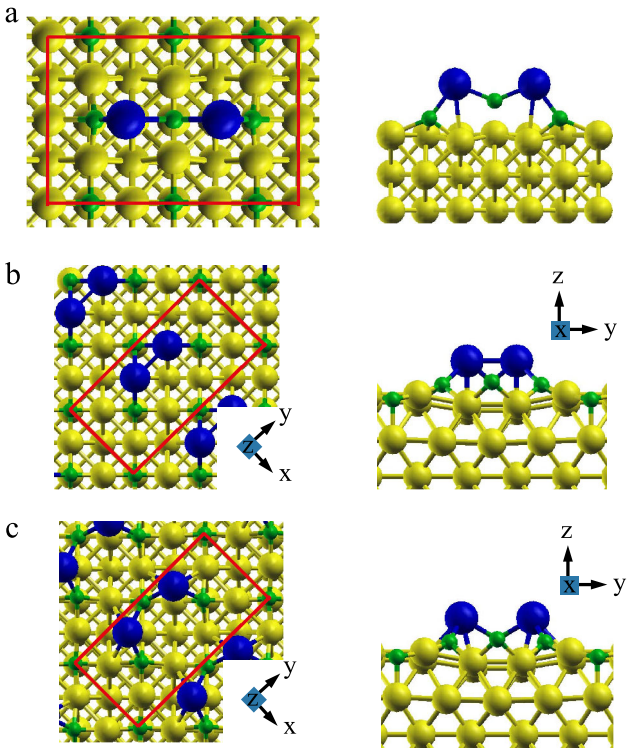

FIG. 2. (a) The top view and along-dimer side view of the relaxed linear Gd dimer on the CuN surface. (b),(c) Structural views similar to (a) for the initial (b) and relaxed diagonal (c) Gd dimers. All in-plane unit cells are marked by red rectangles. In all figures: blue, green, and yellow balls denote Gd, N, and Cu atoms, respectively.

III. RESULTS AND DISCUSSIONS

A. Structure geometry and Gd spin

We therefore arrange Gd atoms in those two geometries on the CuN surface, and optimize the crystal structures until the maximum force among all the atoms reduces to approximately less than 10 mRy/a_0 and 5 mRy/a_0 [26], respectively. The relaxed structures are shown in Fig. 2, and the dimer local geometries are quantitatively presented in Table I. It is interesting to note that the diagonal Gd dimer relaxes its bond angle from 90° to 112°. This change can be understood given that the diagonal Gd-to-Gd distance in GdN bulk is 3.52 Å, and the initial Gd-Gd distance on the surface is 2.56 Å, much shorter than 3.52 Å, so a relaxed Gd-Gd distance on the surface of 3.64 Å is rather reasonable. To determine the Gd spin on the CuN surface, we plot the calculated partial density of states (PDOS) of a single Gd on the CuN surface in Fig. 3. One clearly sees that the $4f$ majority spin states are all occupied and the minority states are all unoccupied, which implies a $4f^7$ configuration for Gd, and a spin-7/2 configuration for its $4f$ shell. In addition, the $5d$ states are not occupied, and its rather small PDOS in the entire energy range indicates its delocalization outside of the Gd atomic sphere, in contrast to a free Gd atom that carries a valence configuration of $5d^1 4f^7 6s^2$. By comparing the Gd2/CuN and the GdN bulk, we find that both systems have each Gd atom connecting to N atoms such that their Gd local structures are very similar to each other but are significantly different to the structure of a free atom. The local structure plays an

TABLE I. Gd-to-Gd distances, Gd-N bond length, Gd-N-Gd bond angle, and the spin coupling J between Gd, calculated for four systems. The Gd dimers are placed on the CuN surface.

	Gd to Gd (Å)	Gd-N (Å)	∠Gd-N-Gd	J (meV)
NN Gd in GdN bulk	3.52	2.49	90°	−1.51
Next-NN Gd in GdN bulk	4.98	2.49	180°	1.09
Diagonal Gd dimer	3.64	2.19	112°	−1.25
Linear Gd dimer	4.15	2.24	135°	1.24

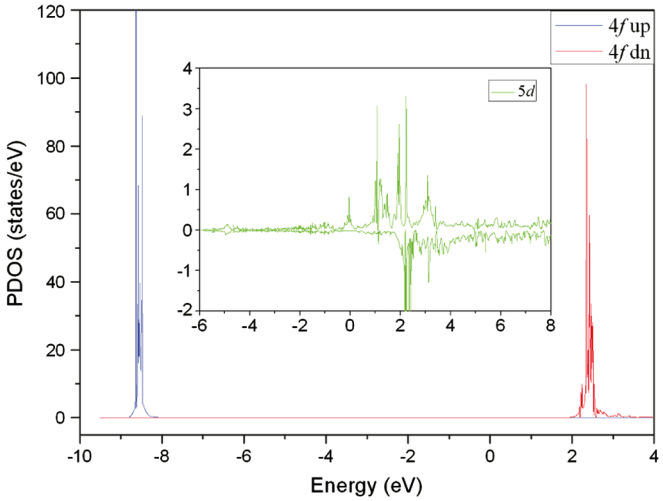

FIG. 3. Partial density of states of a single Gd on the CuN surface.

important role in the spins of all three Gd-contained systems. The anisotropy energy of Gd at the Cu site of the CuN surface can be calculated by pointing the Gd spin in the hollow, N-row, and out-of-plane three symmetry directions by including the spin-orbit coupling. We calculate the lowest- and highest-energy spin directions to be out-of-plane and hollow. The energy differences are calculated to be 0.02 meV between the hollow and N row and 0.09 meV between the N row and out-of-plane, which are tiny, as expected from the $L = 0$ f shell of Gd.

B. Interatomic magnetic interaction

To calculate the spin coupling J between Gd spins on the CuN surface, we take advantage of the correspondence between the collinear spins of a Heisenberg model and the magnetic moments of the real crystal surface of interest [19]. The Hamiltonian of a Heisenberg spin dimer is

$$H = J\mathbf{S}_1 \cdot \mathbf{S}_2. \tag{1}$$

The difference of energy expectation values δE between the parallel and antiparallel spins is related to the coupling J, for spin-S atoms, as

$$\delta E = JS^2 - (-JS^2) = 2JS^2. \tag{2}$$

By calculating the total energies of the parallel- and antiparallel-spin configurations of a Gd dimer at the Cu site of a CuN surface, we obtain from (2) the exchange coupling J of 1.24 meV for the linear dimer and -1.25 meV for the diagonal dimer. Our calculations obtain an antiferromagnetic coupling for the linear Gd dimer and ferromagnetic for the diagonal dimer. One can also see in Table I a trend that the coupling J varies with the angle ∠Gd-N-Gd. The two Gd atoms start with a ferromagnetic coupling at an exact right angle, which becomes slightly less ferromagnetic at ∠Gd-N-Gd = 112°, changes to antiferromagnetic at ∠Gd-N-Gd = 135°, and finally stays antiferromagnetic when along a straight line.

C. Direct exchange, superexchange, and RKKY interaction

We now turn our attention to the underlying mechanism of the ferromagnetism (antiferromagnetism) of the diagonal (linear) Gd dimer. Three possible magnetic interactions may couple the two Gd spins: direct exchange, superexchange, and the RKKY interaction. To extract the three components out of the resultant coupling, we perform calculations of two alternative model systems. One is the original Gd dimer on the surface with the in-between N atom replaced by an Ne atom, which effectively turns off the superexchange. The other is a Gd dimer on top of a single CuN monolayer, i.e., we remove the underlying metallic Cu(100) slab, with the dimer and CuN sheet remaining, which have basically no RKKY interaction. The atomic positions of these two alternative model systems exactly follow the original realistic surface, i.e., their structures are not relaxed, so that the magnetic coupling is the only difference among these systems. We then decompose the spin couplings of the three systems: the original Gd dimer on the CuN/Cu(100) surface J, the one with an Ne between two Gd atoms J_α, and the Gd dimer on a single CuN sheet J_β, into the contributions of direct exchange J_d, superexchange J_s, and RKKY J_r. We write their relations as

$$J = J_\mathrm{d} + J_\mathrm{s} + J_\mathrm{r}, \qquad J_\alpha = J_\mathrm{d} + J_\mathrm{r}, \qquad J_\beta = J_\mathrm{d} + J_\mathrm{s}. \tag{3}$$

It is a simple matter to solve for J_d, J_s, and J_r. The calculated spin couplings are listed in Table II.

For the diagonal dimer, the insignificant differences among J, J_α, and J_β imply that the N atom in between and the underlying conduction electrons play minor roles in the spin coupling of the Gd dimers, while the direct wave function overlapping between the two Gd atoms actually dominates. In fact, the obtained J_d, J_s, and J_r values of the diagonal dimer reflect the statement above, where the superexchange and RKKY are 34% and 5% of the direct

TABLE II. Calculated spin couplings in meV of the original Gd dimers on the CuN/Cu(100) surface J; the Gd dimers on a single CuN sheet J_β; and the spin coupling for the case in which an Ne atom J_α is substituted for the N between the Gd . Also listed are direct exchange J_d, superexchange J_s, and RKKY J_r extracted from J, J_α, and J_β.

	J	J_α	J_β	J_d	J_s	J_r
Diagonal	−1.25	−0.92	−1.30	−0.97	−0.33	0.05
Linear	1.24	−0.88	0.66	−1.46	2.12	0.58

exchange, respectively. Notably, we find a ferromagnetic superexchange. The linear dimer, on the other hand, has quite different components of the three types of magnetic couplings. Antiferromagnetic superexchange dominates, larger than the direct exchange, and there is also significant antiferromagnetic RKKY, at 27% of superexchange. When comparing the same types of magnetic interaction between the two dimer geometries, we find that the direct exchanges of both dimers have the same sign and order of magnitude, while the superexchanges, J_s, of both dimers have opposite signs. Consequently, the magnitude of J_s determines the sign of the dimers' total J. With the knowledge that the ferromagnetic coupling for the diagonal case is partly due to ferromagnetic superexchange, we revisit Table I, and interpret the trend that the coupling J varies with the angle ∠Gd-N-Gd as a rough measure of the angle dependence of superexchange in these systems. The prediction of ferromagnetic superexchange at 90°, varying through a sign change, and ending up at antiferromagnetic for 180° is well known in the chemistry community [27]; it is due to different orbitals being involved with the superexchange hopping to the N at different angles. Pauli exclusion favors antiferromagnetic coupling only when the three atoms are more or less in a line. At sharper angles, the relative symmetries of the orbitals involved in the hopping through the N tend to favor ferromagnetic alignment of the spins.

D. Spin density

In order to obtain more physical insights for the Gd dimers, we plot their spin densities for both the parallel-spin and antiparallel-spin configurations in Fig. 4. The parallel-spin configuration of a diagonal dimer has its spin density forming one isosurface lobe [Fig. 4(a)], while the antiparallel-spin has two disconnected Gd lobes of opposite spins [Fig. 4(b)]. In the ferromagnetic configuration, the intermediate N spin is partially enveloped by the Gd-dimer spin lobe and is carrying an oppositely polarized spin. In the antiferromagnetic configuration, the N atom in between becomes a magnetic dipole antisymmetrically polarized by the two opposite Gd spins. We compare this spin density with that of a linear Gd dimer on the same surface in Figs. 4(c) and 4(d). We see that, while the ferromagnetic diagonal dimer has its two connected spin lobes, the ferromagnetic linear dimer forms two disjoint ones. The linear dimer has an antiferromagnetic ground state, and the corresponding spin density has a nodal plane exactly in the middle of the two Gd. Direct spin interchange in the linear case is expected to be less strong because of the intervening nitrogen and compared to the "spin bonding" between the two Gd atoms in the diagonal case, the latter implying a strong overlapping of their spin unpaired orbitals. However, from Table II, we see that the linear case has direct exchange 1.5 times that of the diagonal.

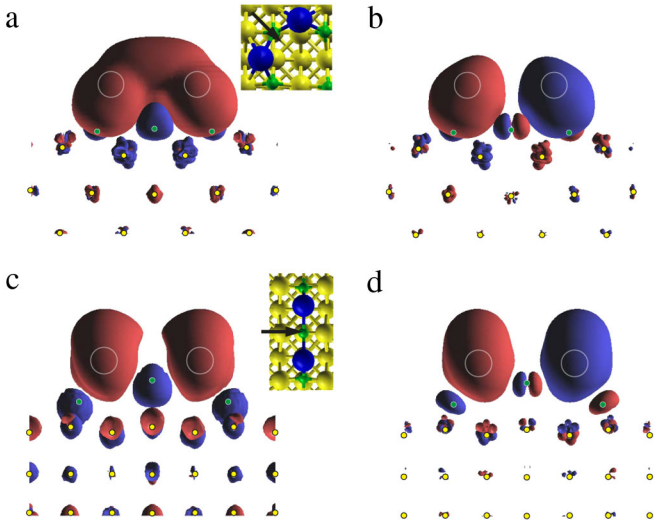

FIG. 4. Calculated spin-density isosurfaces of diagonal and linear Gd dimers on CuN in their ferromagnetic and antiferromagnetic configurations. (a),(b) The side views of the ferromagnetic and antiferromagnetic diagonal dimers. (c),(d) The side views of the ferromagnetic and antiferromagnetic linear dimers. Red stands for positive magnetization, and blue for negative. The open white circles indicate the muffin-tin spheres of the Gd atoms. The black arrow in the stickball inset of each plot indicates the observation direction. The green and yellow solid circles denote the positions of N and Cu atoms, respectively. All spin densities are plotted at the magnitude of $0.001e/a_0^3$, where a_0 is the Bohr radius.

In order to understand the physics underlying the direct exchange in these two configurations, we set out to isolate the direct exchange. The strong superexchange of the linear dimer results in an antiferromagnetic ground state, and the dimer has a fundamental nodal plane in the middle, which obscures the underlying direct exchange in the spin density. To eliminate the superexchange from the system, we study instead our model systems with N replaced by Ne. Both superexchange-free configurations exhibit a ferromagnetic ground state, which we attribute to the underlying direct exchange. We plot their ferromagnetic spin densities in Fig. 5. The diagonal Gd-Ne-Gd dimer [Figs. 5(a) and 5(b)] has a spin-density lobe very similar to that of a realistic Gd dimer, which is consistent with the dominant direct exchange seen in Table II. The linear Gd-Ne-Gd dimer [Figs. 5(c) and 5(d)], on the other hand, provides new information from its shape. We see a negative spin lobe exactly in the middle, together with prolongation of positive polarization perpendicular to the dimer, as viewed from the top. In both configurations, we see the strong effect of orbital symmetry in the interactions. In the diagonal case, there are no nodes, and, in the linear case, we see that there are two nodes, with a small maximum in the middle. This strong indication of orbital interaction is further confirmation that we are seeing direct exchange.

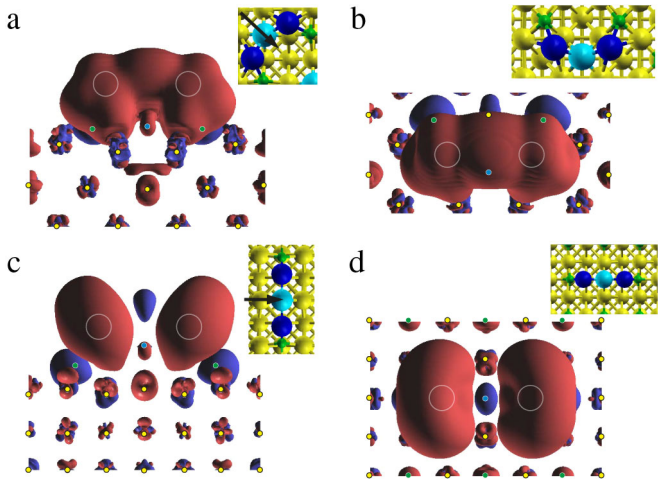

FIG. 5. Calculated spin-density isosurfaces of the modeled Gd dimers on CuN with the in-between N replaced by Ne. Such dimers are called the Gd-Ne-Gd dimer later, and both are in their ferromagnetic configuration here. (a),(b) The side and top views of the diagonal dimer. (c),(d) The side and top views of the linear dimer. For all four plots, red stands for positive magnetization, and blue for negative. The open white circles indicate the muffin-tin spheres of the Gd atoms. Stickball insets of each plot show atomic positions, with the black arrows for the side views indicating the observation direction. The green, yellow, and light blue solid circles denote the positions of N, Cu, and Ne, respectively. All spin densities are plotted at the magnitude of $0.0005e/a_0^3$.

E. Spin-dependent partial density of states

In order to further understand the details of the interstitial spin density between the Gd atoms of the diagonal dimer, we plot the spin-dependent partial density of states (S-PDOS) in the entire interstitial region of the unit cell [Fig. 6(a)]. (S-PDOS is defined as the minority-spin DOS subtracted from the majority-spin DOS in this region.) There is an isolated positive peak at $E = -9$ eV, which is exactly the energy of the majority-spin $4f$ level. The highly oscillating S-PDOS within the energy range from $E = -8$ to -1 eV results in the spins of the majority- and minority-spin orbitals approximately cancelling. In contrast, from $E = -1$ eV to the Fermi energy, the S-PDOS shows a peak that dominates, labeled D_1. D_1 actually represents three equivalent near-energy peaks. There are also two other peaks in region A. In Fig. 6(c), left image, we plot the majority-spin probability density of D_1. We can see that the highest probability of D_1 is mainly concentrated in the interstitial region between two Gd and provides the major contribution to the interstitial spin density. Although we do not plot the other two near-energy peaks here, we have found that they look very similar. In contrast, all other peaks, positive and negative, in region A have negligible weight between the two Gd and represent the interstitial electrons in the bulk Cu. The interstitial contribution of D_1 is decomposed into plane waves in the full-potential-linearized-augmented-plane-wave basis. To trace

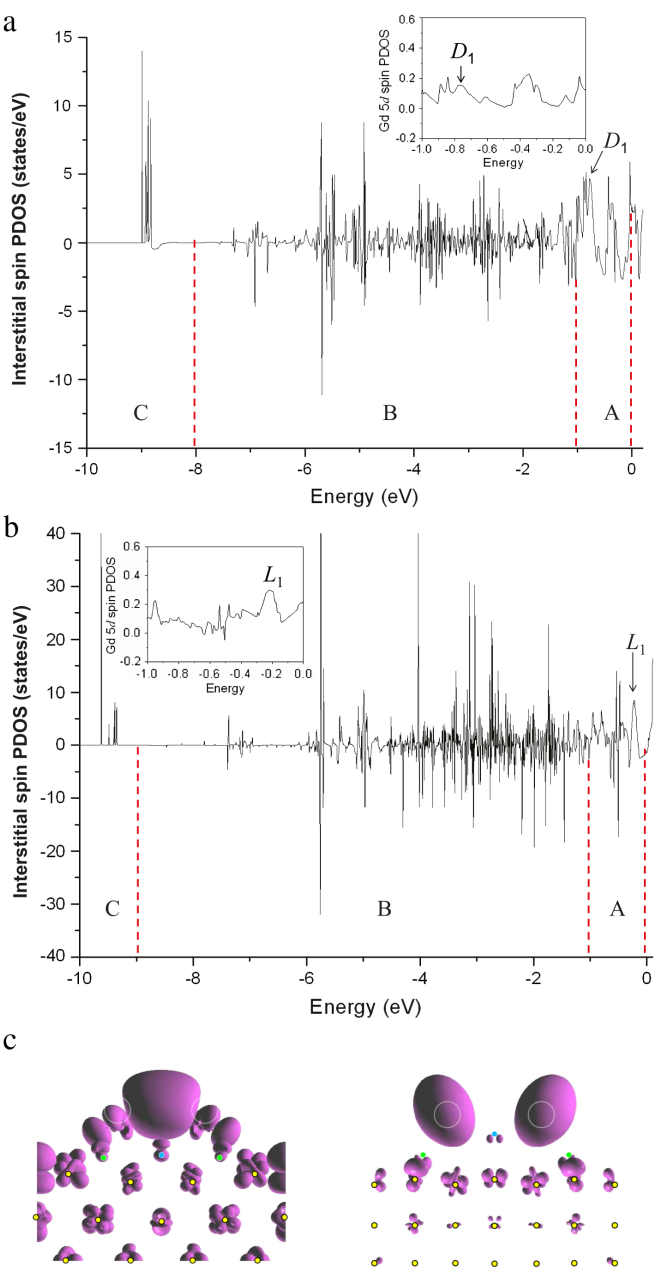

FIG. 6. (a) Spin-dependent partial density of states (S-PDOS) in the entire interstitial region of a ferromagnetic diagonal Gd-Ne-Gd dimer on CuN, defined as the majority-spin DOS minus the minority-spin in this spatial region. The plotted energy range is divided into three regions. Region A: The S-PDOS is mostly positive. The peak that dominates the S-PDOS is labeled D_1. Region B: The S-PDOS is highly oscillating. Region C: A single positive peak at the energy of the majority-spin $4f$ level. The inset shows the Gd $5d$ S-PDOS in the energy range A. (b) Same plots as (a) for the linear Gd-Ne-Gd dimer. The dominating peak is labeled L_1. (c) The majority-spin probability densities of the orbitals D_1 (left) and L_1 (right), viewed along the same orientation as the side view of the spin density of the diagonal and linear Gd-Ne-Gd dimers in Figs. 5(b) and 5(d), respectively. The open white circles indicate the muffin-tin spheres of the Gd atoms. The isosurfaces are plotted at the value of $0.02a_0^{-3}$.

the atomic configuration of the above interstitial spin between the Gd, we calculate the projections of the D_1 orbital to s, p, and d symmetries within a Gd muffin-tin sphere. (There is no appreciable f DOS in the interstitial region.) The calculated muffin-tin projections to $6s$, $6p$, and $5d$ are 17%, 13.5%, and 68.5% of Gd, respectively. We also plot the Gd $5d$ S-PDOS around the D_1 energy, and find that there is also a peak exactly at D_1. Consequently, we believe that the Gd $5d$ electrons are delocalized across the diagonal to enable the direct exchange.

We also perform S-PDOS analysis for the linear Gd-Ne-Gd dimer, and plot it in Fig. 6(b). The linear-dimer S-PDOS can be analyzed in a manner similar to that of the diagonal. There are a number of peaks in region A. However, the peak that dominates the S-PDOS surrounding the Gd is the one which we label L_1 in the figure. Unlike the diagonal Gd-Ne-Gd dimer, the L_1 peak has a wide width and does not have energy neighbors. The majority-spin probability is also different from D_1 and is elongated on the surface perpendicularly to the Gd-Gd direction, very similar to Fig. 5(d). As seen in Fig. 6(c), right image, we notice that the two Gd orbital lobes of L_1, unlike D_1, do not connect with each other, and instead have a node in between and an antibonding appearance.

As calculated for D_1, the muffin-tin projections of L_1 to Gd $6s$, $6p$, and $5d$ are 33%, 3%, and 64% of Gd, respectively. The $5d$ character of L_1 within the Gd muffin-tin sphere is consistent with the $5d$ S-PDOS plotted in the inset of Fig. 6(b). Therefore, we also believe that the Gd $5d$ electrons, as in the diagonal case, are delocalized to enable the direct exchange of the linear dimer. The spreading of L_1 out of the Gd muffin-tin spheres into the interstitial region represents 54% of the total probability distribution, while D_1 plus its two near-energy neighbors represent only 43%. We see that the linear configuration has a contribution roughly 1.3 times that of the diagonal, a ratio close to the 1.5 ratio between the direct exchange couplings of the two configurations shown in Table II. In fact, if we quantify the interstitial magnetic moments of the diagonal and linear Gd-Ne-Gd dimers, they are 1.53 and 2.34, respectively, with a ratio of 1.54, even closer to 1.5. The absence and presence of a middle nodal plane between the two geometries of the Gd-Ne-Gd dimers are very likely due to the symmetry of their (hybridized) delocalized Gd orbitals, a coupling we refer to generically as "spin bonding."

F. GdN bulk

We now consider bulk GdN. A natural generalization of the spin bonding of the diagonal-dimer direct exchange is to ask whether the ferromagnetic NN coupling in a GdN bulk is, like the diagonal Gd dimer, also related to a spin bonding. For this, we plot the spin density of the GdN bulk in Fig. 7(a), where it can clearly be seen that there is no obvious spin-density lobe connecting two Gd atoms, i.e., no spin bonding in a GdN bulk. In fact, a previous DFT

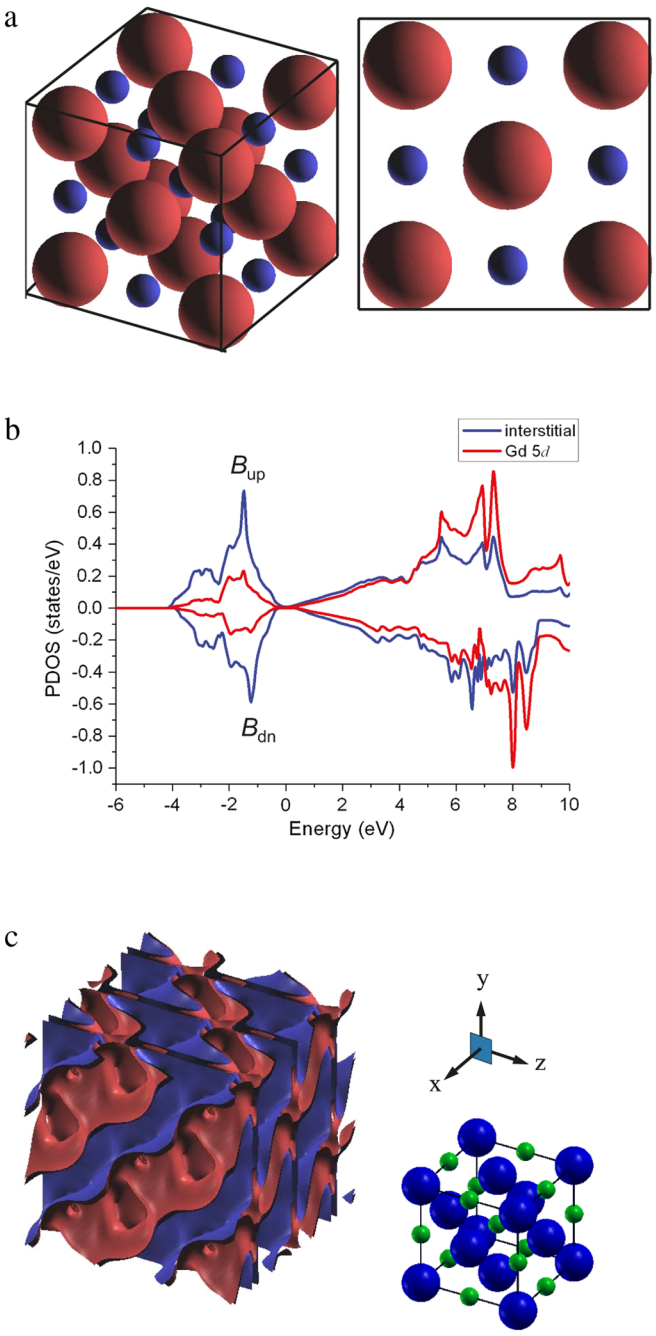

FIG. 7. (a) Calculated spin-density isosurfaces of a GdN bulk. The right plot is viewed along the direction perpendicular to a cube face and has the isosurfaces of only the nearest atoms plotted for better visualization. The plotted region represents a GdN conventional unit cell extended by 30% of the lattice constant, so that the spin isosurfaces of atoms at face centers and corners can be entirely plotted. Red stands for positive spin polarization, and blue for negative. Gd and N atoms have nearly spherical positive and negative isosurfaces, respectively. (b) Interstitial and Gd $5d$ PDOS of a ferromagnetic GdN bulk. The main peaks of occupied majority- and minority-spin PDOS are labeled B_{up} and B_{dn}, respectively. (c) Isosurface of the spin probability density of the PDOS peak at the value of $0.0002a_0^{-3}$.

study of GdN [23] has already concluded that the ferromagnetism of the diagonal nearest neighbors most likely originates from the RKKY interaction; the authors of [23] analyzed the trends of exchange coupling of differently strained GdN compared to all other gadolinium pnictides of larger-size anions. RKKY is quite prominent in Gd bulk compounds, compared to a pair of surface adatoms, because of the increased free-electron density of states contributed by all of the Gd. As we will show in the next paragraph, the oscillating spin density in the interstitial region makes direct exchange much less likely in the bulk.

To understand how Gd spins couple to each other through their delocalized electrons in a GdN bulk, we plot both the interstitial and 5*d* PDOS. This coupling is shown in Fig. 7(b). Within 5 eV below the Fermi energy, the main PDOS peak around $E = -1.2$ eV has a significant interstitial component but only a minor 5*d*. We further plot both the majority- and minority-spin orbitals associated with this peak, shown in Fig. 7(c). The isosurfaces of the orbitals spread over all the interstitial region. This can be interpreted as follows: The Gd 5*d* electrons in the GdN bulk join the conduction electron sea, and consequently they contribute to the RKKY interactions but they do not form a directional orbital interaction in between two Gd as in the surface dimer case. Although the ferromagnetism seems to be understood quite well by RKKY interaction, the GdN-bulk study [23] does not exclude the possibility of a ferromagnetic contribution from the 90°-superexchange interaction, which those authors note can be quite large in some oxides. Indeed, from our finding of superexchange that becomes ferromagnetic at an angle of 112°, we predict that the 90° coupling in bulk material has at least some ferromagnetic superexchange as well.

IV. CONCLUSIONS

In summary, we have calculated the electronic structure of coupled rare-earth (Gd) spins on a surface using the PBE + U exchange correlation, in the first study of rare-earth spin-coupled adatoms. The presence of Gd gives rise to a rearrangement of the atomic structure that is quite different from that of a Mn atom [19]. The geometry effect of the spin coupling is manifested by calculating the exchange coupling between Gd atoms on the CuN surface and finding antiferromagnetic coupling in a linear geometry and ferromagnetic in a diagonal geometry, showing that the sign of J can be tuned by different angular arrangements, with roughly the same magnitude. We also find that the Gd dimers in these two geometries have many similarities to the nearest-neighbor (NN) and the next-NN Gd atoms in a GdN bulk.

The underlying physics of the dimers' magnetism is studied by decomposing the magnetic couplings into the direct exchange, superexchange, and RKKY interaction, using our new methodology. The strength of the direct exchange is further pictorially understood by the "spin bonding" between two Gd atoms, by extracting the relevant wave functions in a configuration which excludes competing superexchange and RKKY effects. This analysis shows that, while the atomic magnetism for Gd is due to the localized f electrons, the direct exchange between two Gd is due to their d electrons, which have become itinerant. We find that the diagonal case has ferromagnetic contributions from both direct exchange and superexchange. The antiferromagnetism for the linear geometry is due to the predominance of superexchange for this configuration, notwithstanding a large ferromagnetic direct exchange. Superexchange is present in both geometries for the Gd dimer: ferromagnetic for the diagonal and antiferromagnetic for the linear. Even for the ferromagnetic coupling of the diagonal dimer, superexchange constitutes 27% of the total interaction. We note a trend that the sign of superexchange changes with angle, consistent with previous predictions in the chemistry community. While the bulk GdN compound is basically dominated by RKKY interactions, we find much smaller but still nonzero RKKY interactions with the Gd dimers on a CuN surface, with a nontrivial contribution of RKKYinteractions, particularly in the linear configuration. This is the first reported RKKY interaction of engineered magnetic atoms on insulating surfaces. Our calculations also show that the Gd spin of these structures is 7/2, the same as that of GdN bulk, but different from a spin-4 free Gd atom with a valance configuration of $4f^7 5d^1 6s^2$.

ACKNOWLEDGMENTS

We thank S. Loth, A. Heinrich, and J. Gupta for stimulating discussions. C.-Y. L acknowledges financial support from the Taiwan National Science Council (under Grant No. NSC 97-2112-M-009-007-MY3), the National Chiao Tung University Ministry-of-Education Aiming-for-Top-University Program, and Taiwan National Center for Theoretical Sciences, and facility support from the Taiwan National Center for High-performance Computing. B. A J. acknowledges that this material is based upon work supported in part by the National Science Foundation under Grant No. 1066293 and the hospitality of the Aspen Center for Physics.

[1] J. R. Petta, A. C. Johnson, J. M. Taylor, E. A. Laird, A. Yacoby, M. D. Lukin, C. M. Marcus, M. P. Hanson, and A. C. Gossard, *Coherent Manipulation of Coupled Electron Spins in Semiconductor Quantum Dots*, Science **309**, 2180 (2005).

[2] R. Wiesendanger, *Spin Mapping at the Nanoscale and Atomic Scale*, Rev. Mod. Phys. **81**, 1495 (2009), and references therein.

[3] C. F. Hirjibehedin, C. P. Lutz, and A. J. Heinrich, *Spin Coupling in Engineered Atomic Structures*, Science **312**, 1021 (2006).

[4] P. Wahl, P. Simon, L. Diekhöner, V. S. Stepanyuk, P. Bruno, M. A. Schneider, and K. Kern, *Exchange Interaction between Single Magnetic Adatoms*, Phys. Rev. Lett. **98**, 056601 (2007).

[5] F. Meier, L. Zhou, J. Wiebe, and R. Wiesendanger, *Revealing Magnetic Interactions from Single-Atom Magnetization Curves*, Science **320**, 82 (2008).

[6] L. Zhou, J. Wiebe, S. Lounis, E. Vedmedenko, F. Meier, S. Blügel, P. H. Dederichs, and R. Wiesendanger, *Strength and Directionality of Surface Ruderman-Kittel-Kasuya-Yosida Interaction Mapped on the Atomic Scale*, Nature Phys. **6**, 187 (2010).

[7] C. F. Hirjibehedin, C.-Y. Lin, A. F. Otte, M. Ternes, C. P. Lutz, B. A. Jones, and A. J. Heinrich, *Large Magnetic Anisotropy of a Single Atomic Spin Embedded in a Surface Molecular Network*, Science **317**, 1199 (2007).

[8] D. Serrate, P. Ferriani, Y. Yoshida, S.-W. Hla, M. Menzel, K. von Bergmann, S. Heinze, A. Kubetzka, and R. Wiesendanger, *Imaging and Manipulating the Spin Direction of Individual Atoms*, Nature Nanotech. **5**, 350 (2010).

[9] S. Loth, M. Etzkorn, C. P. Lutz, D. M. Eigler, and A. J. Heinrich, *Measurement of Fast Electron Spin Relaxation Times with Atomic Resolution*, Science **329**, 1628 (2010).

[10] A. F. Otte, M. Ternes, K. von Bergmann, S. Loth, H. Brune, C. P. Lutz, C. F. Hirjibehedin, and A. J. Heinrich, *The Role of Magnetic Anisotropy in the Kondo Effect*, Nature Phys. **4**, 847 (2008).

[11] A. F. Otte, M. Ternes, S. Loth, C. P. Lutz, C. F. Hirjibehedin, and A. J. Heinrich, *Spin Excitations of a Kondo-Screened Atom Coupled to a Second Magnetic Atom*, Phys. Rev. Lett. **103**, 107203 (2009).

[12] A. A. Khajetoorians, J. Wiebe, B. Chilian, and R. Wiesendanger, *Realizing All-Spin-Based Logic Operations Atom by Atom*, Science **332**, 1062 (2011).

[13] S. Loth, S. Baumann, C. P. Lutz, D. M. Eigler, and A. J. Heinrich, *Bistability in Atomic-Scale Antiferromagnets*, Science **335**, 196 (2012).

[14] B. Barbara and L. Gunther, *Magnets, Molecules and Quantum Mechanics*, Phys. World **12**, 35 (1999) [http://physicsworldarchive.iop.org/index.cfm?action=summary&doc=12%2F3%2Fphwv12i3a28%40pwa-xml&qt]; D. Gatteschi and R. Sessoli, *Quantum Tunneling of Magnetization and Related Phenomena in Molecular Materials*, Angew. Chem., Int. ed. Engl. **42**, 268 (2003); M. Verdaguer, *Rational Synthesis of Molecular Magnetic Materials: A Tribute to Olivier Kahn*, Polyhedron **20**, 1115 (2001).

[15] J. D. Rinehart and J. R. Long, *Exploiting Single-Ion Anisotropy in the Design of f-Element Single-Molecule Magnets*, Chem. Sci. **2**, 2078 (2011).

[16] C.-G. Duan, R. F. Sabiryanov, W. N. Mei, P. A. Dowben, S. S. Jaswal, and E. Y. Tsymbal, *Magnetic Ordering in Gd Monopnictides: Indirect Exchange versus Superexchange Interaction*, Appl. Phys. Lett. **88**, 182505 (2006).

[17] C. Mitra and W. R. L. Lambrecht, *Magnetic Exchange Interactions in the Gadolinium Pnictides from First Principles*, Phys. Rev. B **78**, 134421 (2008).

[18] O. O. Brovko, P. A. Ignatiev, V. S. Stepanyuk, and P. Bruno, *Tailoring Exchange Interactions in Engineered Nanostructures: An Ab Initio Study*, Phys. Rev. Lett. **101**, 036809 (2008).

[19] C. Y. Lin and B. A. Jones, *First-Principles Calculations of Engineered Surface Spin Structures*, Phys. Rev. B **83**, 014413 (2011).

[20] J. P. Perdew, K. Burke, and M. Ernzerhof, *Generalized Gradient Approximation Made Simple*, Phys. Rev. Lett. **77**, 3865 (1996).

[21] P. Blaha, K. Schwarz, G. Madsen, D. Kvasnicka, and J. Luitz, *Computer Code WIEN2K: An Augmented Plane Wave plus Local Orbitals Program for Calculating Crystal Properties* (Vienna University of Technology, Vienna, 2001).

[22] A. I. Liechtenstein, V. I. Anisimov, and J. Zaanen, *Density-Functional Theory and Strong Interactions: Orbital Ordering in Mott-Hubbard Insulators*, Phys. Rev. B **52**, R5467 (1995).

[23] C.-G. Duan, R. F. Sabiryanov, J. Liu, W. N. Mei, P. A. Dowben, and J. R. Hardy, *Strain Induced Half-Metal to Semiconductor Transition in GdN*, Phys. Rev. Lett. **94**, 237201 (2005).

[24] C. Waldfried, D. N. McIlroy, D. Li, J. Pearson, S. D. Bader, and P. A. Dowben, *Dissociative Nitrogen Chemisorption and Bonding on Gd(0001)*, Surf. Sci. **341**, L1072 (1995).

[25] F. Leuenberger, A. Parge, W. Felsch, K. Fauth, and M. Hessler, *GdN Thin Films: Bulk and Local Electronic and Magnetic Properties*, Phys. Rev. B **72**, 014427 (2005).

[26] Here we briefly summarize certain computational details: The numbers of k points used are $4 \times 2 \times 1$ and $3 \times 2 \times 1$ for the diagonal and linear dimers, respectively. The convergence of J with respect to k points is less than 6%. The slab configuration was checked in a previous work [19], showing that a five-layer slab is thick enough. We also test U and J_f by varying them away from the bulk-GdN values as large as $U = 11$ and $J_f = 1.4$ eV, and find that the spin couplings become -1.26 and 1.36 meV for the diagonal and linear dimers, respectively.

[27] A. Bencini and D. Gatteschi, *EPR Exchange Coupled Systems* (Springer Verlag, Berlin, 1990); see also R. Pushpa, J. Cruz, and B. Jones, *Spin and Exchange Coupling for Ti Embedded in a Surface Dipolar Network*, Phys. Rev. B **84**, 075422 (2011).